

# A Physical Interpretation of Imaginary Time Delay

Isabella L. Giovannelli\* and Steven M. Anlage  
Maryland Quantum Materials Center, Department of Physics  
University of Maryland, College Park, Maryland 20742, USA  
(Dated: December 18, 2024)

The scattering matrix  $S$  linearly relates the vector of incoming waves to outgoing wave excitations, and contains an enormous amount of information about the scattering system and its connections to the scattering channels. Time delay is one way to extract information from  $S$ , and the transmission time delay  $\tau_T$  is a complex (even for Hermitian systems with unitary scattering matrices) measure of how long a wave excitation lingers before being transmitted. The real part of  $\tau_T$  is a well-studied quantity, but the imaginary part of  $\tau_T$  has not been systematically examined experimentally, and theoretical predictions for its behavior have not been tested. Here we experimentally test the predictions of Asano, *et al.* [Nat. Comm. **7**, 13488 (2016)] for the imaginary part of transmission time delay in a non-unitary scattering system. We utilize Gaussian time-domain pulses scattering from a 2-port microwave graph supporting a series of well-isolated absorptive modes to show that the carrier frequency of the pulses is changed in the scattering process by an amount in agreement with the imaginary part of the independently determined complex transmission time delay,  $\text{Im}[\tau_T]$ , from frequency-domain measurements of the sub-unitary  $S$  matrix. Our results also generalize and extend those of Asano, *et al.*, establishing a means to predict pulse propagation properties of non-Hermitian systems over a broad range of conditions.

**Introduction.** In linear scattering systems, the scattering matrix  $S$  is used to relate incoming waves  $|\psi_{in}\rangle$  to outgoing waves  $|\psi_{out}\rangle$  where  $|\psi_{out}\rangle = S|\psi_{in}\rangle$ . The scattering matrix  $S$  is a complex function of energy (or frequency) and is a square  $M \times M$  matrix where  $M$  is the number of channels coupling the system to the outside world. This formulation of scattering as well as its statistical treatment using random matrix theory [1–9] can be applied to a wide array of complex systems. A non-exhaustive list includes: microwave and sound scattering experiments [10–16], nuclear and atomic scattering [5], and scattering in quantum many-body systems [17]. The scattering matrix encapsulates a vast amount of information regarding the scattering system [5, 18–20]. It can be used to determine how long a wave stays in the scattering system before leaving, which is referred to as time delay.

In the same way that the scattering matrix can be used to describe a broad range of scattering phenomena, time delay is just as widely applicable. In quantum mechanics, time delay is directly related to the phase evolution of quantum waves [21, 22]. It can also be related to the density of states of open scattering systems [23, 24]. In photonics, time delay can be used to determine group delay in optical fibers and manipulate the shape of wavefronts [25–29]. The time delay operator can also be utilized to optimize light storage within disordered media [30], and to characterize scattering of narrow-band acoustic pulses [31]. In electromagnetics, time delay can be used to determine group delay in wave guides [32–34] and to control the level of energy focused within a microwave enclosure [35]. It can also be used to determine the locations of poles and zeros of the scattering matrix in the complex

frequency plane [7, 36–40].

## Time Delay in Unitary Scattering Systems.

Time delay was first described by Eisenbud [41] and Wigner [42] in the context of elastic nuclear scattering. They defined time delay as the derivative of the wavefunction’s scattering phase shift with respect to energy. This concept was later generalized by Smith [43] to include inelastic scattering and systems with many channels. In the case of classical electromagnetic waves, the setting for the experimental results in this paper, time delay is related to the derivative of the classical wave’s scattering phase shift with respect to frequency [10, 24, 44]. Written in terms of the frequency dependent scattering matrix, the Wigner-Smith time delay for electromagnetic waves is  $\tau_W(\omega) = -\frac{i}{M} \frac{d}{d\omega} \ln[\det S(\omega)]$  where  $\omega$  is angular frequency.

The statistical properties of time delay in highly-overmoded unitary scattering systems have been investigated in detail [7, 45–58], including its use in quantum transport theory [59]. We note that furtive attempts to define a complex generalization of time delay in the context of tunneling [60, 61] have proven to be of limited physical utility [62].

## Time Delay in Subunitary Scattering Systems.

In this paper, we will focus on the time delay associated with the transmission components of the scattering matrix referred to as transmission time delay ( $\tau_T$ ). This is in contrast to Wigner-Smith time delay which is associated with the entire scattering matrix. Since we study a two-port ring graph, the scattering matrix is rank 2:

$S = \begin{pmatrix} R & T' \\ T & R' \end{pmatrix}$  where  $T$  and  $T'$  are the transmission coefficients and  $R$  and  $R'$  are the reflection coefficients.

\* igiovann@umd.edu

Transmission time delay ( $\tau_T$ ) is defined generally as [40],

$$\tau_T(\omega; \alpha) = -i \frac{\partial}{\partial \omega} \ln[\det T(\omega + i\alpha)] = \text{Re}[\tau_T] + i \text{Im}[\tau_T] \quad (1)$$

where here  $T = |S_{21}|e^{i\phi}$ , and  $\alpha$  quantifies the uniform loss in the system. Transmission time delay can be analogously defined for  $T'$  and can be re-written in terms of the S-matrix poles, and the zeros of the transmission sub-matrix, as shown in Refs. [40, 63].

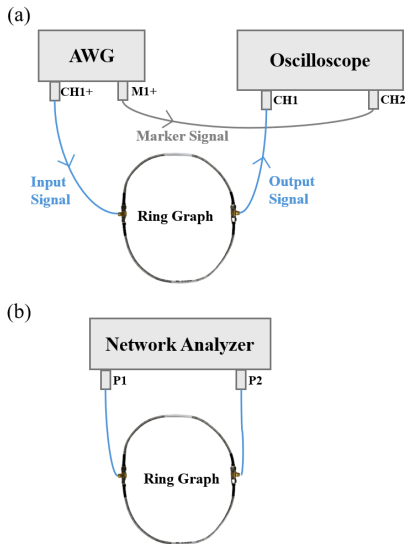


FIG. 1. (a) Schematic of time domain experiments performed. (b) Schematic of the frequency domain experiments performed.

The transmission sub-matrix  $T$  is sub-unitary, hence  $\tau_T$  is complex valued, and its real and an imaginary parts can be either positive or negative. This naturally leads to the question of how to physically interpret this quantity? (See Section VI of the Supp. Mat. [64] for more details.) Addressing this question is best done in the time domain rather than the frequency domain since one can directly see the changes to the structure and shape of the pulse in the time domain.

Negative real time delay was examined theoretically by Garrett and McCumber [65] and experimentally demonstrated by Chu and Wong for light pulses interacting with a single isolated absorptive mode [66]. Negative time delay occurs when the group velocity of the pulse surpasses the speed of light  $c$ . They explained this phenomena to be an artifact of pulse reshaping as it travels through a dispersive medium. Essentially, all the frequencies that make up the pulse are not all transmitted equally, leading to shifts in the center of the pulse (Eq. 4) and its leading edge.

Imaginary time delay was first interpreted by Asano *et al.* [67] as a center-frequency shift in the pulse  $D_\omega$  rather than a time shift. They note that this relationship is akin to the one between time delays and Goos-Hänchen

beam shifts, [68, 69] as well as quantum weak measurements [70–75]. They make the theoretical connection between imaginary time delay and pulse center frequency shift but do not present corresponding experimental results. In this paper, we extend this work by presenting the corresponding experimental results demonstrating the relationship between imaginary time delay (determined from frequency-domain scattering matrix data), and pulse center-frequency shift (obtained from time-domain pulse data).

This paper is structured as follows. First, we briefly review the theoretical model describing pulse propagation through dispersive media. We then present the experimental setup, data, and results. These experimental results are directly compared to the predictions made by Asano *et al.* [67], and we discuss how our results generalize theirs.

**Transmission Time Delay and Gaussian Pulse Properties.** To derive the predicted results one can combine methods used in Asano *et al.* [67] and Cao *et al.* [76]. The calculation details are presented in section III of the Supp. Mat. [64]. Here we summarize the highlights. The main assumptions needed are: 1) The frequency bandwidth of the pulse  $\tilde{\Delta}$  is much smaller than the 3-dB linewidth of the resonant mode being studied  $\gamma_{3\text{-dB}}$ , 2) the propagation distance  $z$  through the system satisfies  $z \ll z_\alpha(\gamma_{3\text{-dB}}/\tilde{\Delta})^2$ , [77] where  $z_\alpha$  is the absorption length of the medium.

The predicted shift in transmission time ( $D_t$ ) and center frequency ( $D_\omega$ ) of a transmitted Gaussian pulse is,

$$D_t = \text{Re}[\tau_T(\omega_c; \alpha)] \quad (2) \quad D_\omega = -\tilde{\Delta}^2 \text{Im}[\tau_T(\omega_c; \alpha)] \quad (3)$$

where  $\tilde{\Delta} = \frac{\pi \tilde{\Delta}_\omega}{\sqrt{2 \ln 2}}$  and  $\tilde{\Delta}_\omega$  is the angular frequency bandwidth of the pulse.

**Experiment.** The experiments were performed using a 2-port microwave ring graph as the scattering system. The ring graph is composed of two coaxial cables of different lengths (27.9 and 30.5 cm long) and two T-junctions, and is depicted in both panels of Fig. 1. There are multiple reasons why we found it advantageous to use a ring graph for this experiment. One is that the ring graph has widely spaced and isolated absorptive modes (see Fig. 2(a)), as assumed in theoretical treatments, allowing for straightforward analysis and interpretation. Another reason is because the  $S$ -matrix and complex time delay of the ring graph have already been thoroughly characterized [40, 78, 79]. We note in passing that prior work has demonstrated that time delay of short pulses in microwave graphs contains useful information about the structure of the graph [80, 81].

**Transmission Time Delay Measurements.** To find the transmission time delay, we used the frequency domain experiment setup depicted in Fig. 1(b). Port 1 (P1) of a Keysight N5242A network analyzer (PNA-X) is attached to one end of the ring graph, the other end of

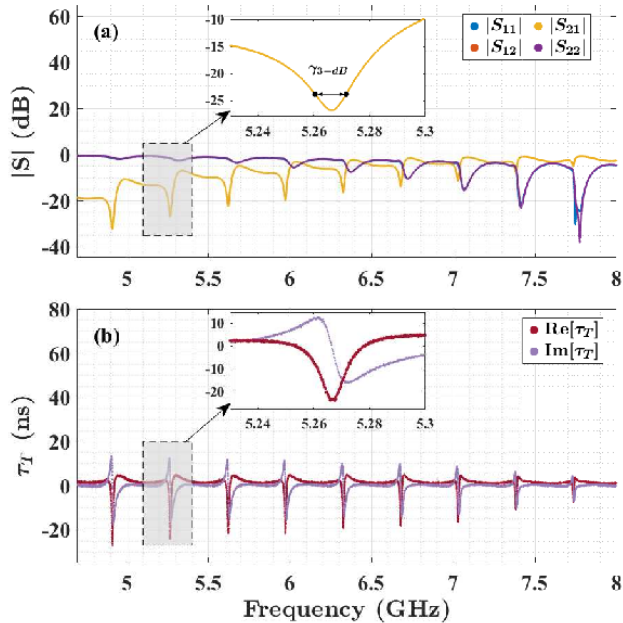


FIG. 2. (a) Measured scattering matrix elements for the ring graph depicted in Fig. 1(b). The transmission parameters are in orange and yellow (overlapping), the reflection parameters are in blue and purple. The inset is a zoomed-in graph of  $S_{21}$  for the indicated boxed region (5.23-5.3 GHz). The 3-dB bandwidth of this resonance is  $\gamma_{3-dB} = 11.15$  MHz. (b) The transmission time delay is calculated using  $S_{21}$  data in (a). The real part is plotted in red and the imaginary part of the transmission time delay is plotted in light purple.

the ring graph is attached to port 2 (P2). The PNA-X is calibrated up to the connection points to the ring-graph with a Keysight N4691-60001 Electronic Calibration kit over the 10 MHz to 18 GHz frequency range with a frequency step size of 179.9 kHz.

Representative frequency domain results are summarized in Fig. 2, where both the measured scattering parameters and the corresponding calculated transmission time delay (using Eq. 1) are depicted as a function of frequency. We see in Fig. 2(a) that the modes are widely spaced without any overlap as characterized experimentally in [40], and assumed theoretically [65, 67].

In Fig. 2(b) we see that both the real and imaginary parts of the transmission time delay evolve through positive and negative values. We also see that the transmission time delay extrema coincide with the scattering resonances.

**Time Domain Gaussian Pulse Measurements.** The time domain measurements were performed using the setup depicted in Fig. 1(a). Channel 1 of a 50 GS/s Tektronix model AWG70001B arbitrary waveform generator (AWG) is attached to one end of the ring graph through a coaxial cable. The other end of the ring graph is attached, using another coaxial cable, to channel 1 of a Keysight/Infiniium model UXR0104A 10-GHz bandwidth real-time digital sampling oscilloscope (DSO). The

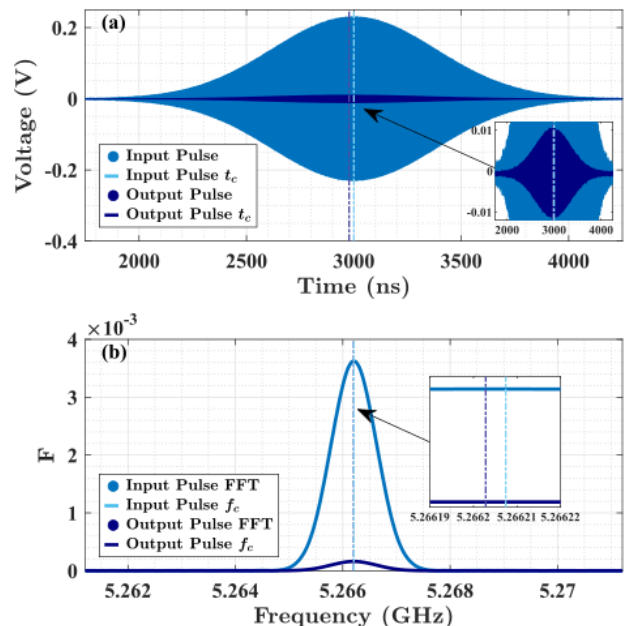


FIG. 3. (a) Example of time domain data for the pulse transmission experiments. The light blue trace is the pulse that is sent into the ring graph. This pulse has a center frequency of 5.2662 GHz and a frequency bandwidth of 1 MHz. The dark blue trace is the output pulse from the ring graph. Their respective transmission times  $t_c$  are plotted as vertical dashed lines. The inset is a zoomed-in plot of the two pulses with a focus on the output pulse. (b) The Fast Fourier Transform of the time domain pulse data shown in (a).

marker channel (M1+) of the AWG is attached to channel 2 of the DSO to trigger the oscilloscope and thus ensure measurements are all taken with the same zero time point. Please see section V in Ref. [64] for details on how the Gaussian pulses were constructed and how the external delay from the cables was taken into account.

In Fig. 3(a) raw time domain data is shown for both the input and output pulses as well as the measured shifts  $\Delta t_c$ ,  $\Delta \omega_c$ . Note that the oscilloscope measures the detailed carrier-frequency oscillations of the pulse and not just its envelope. The input pulse shown here has a center frequency of 5.2662 GHz which situates it right in the center of a resonance of the ring as depicted in the inset in Fig. 2(a). The frequency bandwidth of the pulse is 1 MHz which is significantly smaller than the 3-dB bandwidth of this resonance which is about 11.15 MHz. Since we are working in the small bandwidth limit, we calculate the transmission times ( $t_c$ ) and center frequencies ( $\omega_c$ ) using the first temporal moment of the pulse [82, 83], defined as,

$$t_c = \frac{\int |V(t)|^2 t dt}{\int |V(t)|^2 dt} \quad (4) \quad \omega_c = \frac{\int |F(\omega)|^2 \omega d\omega}{\int |F(\omega)|^2 d\omega} \quad (5)$$

where  $V$  is the voltage,  $t$  is time,  $F$  is the magnitude

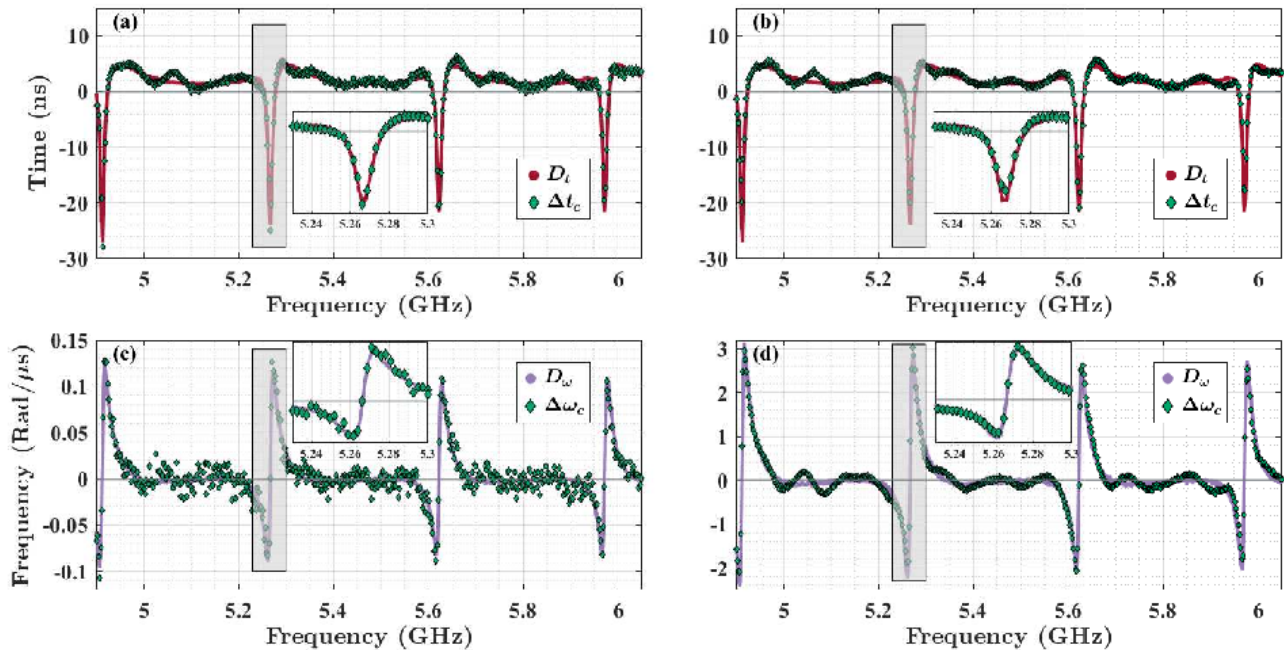


FIG. 4. Results for transmission time and center frequency shifts for an input pulse with a frequency bandwidth of  $\Delta_f = 1$  MHz ((a) and (c)) and a frequency bandwidth of  $\Delta_f = 5$  MHz ((b) and (d)). In (a-b) the red curve corresponds to Eqn. 2. In (c-d) the purple curve corresponds to Eqn. 3. The green diamonds in plots in the top row (bottom row) are time domain experimental data where  $\Delta t_c = t_c^{\text{output}} - t_c^{\text{input}}$  ( $\Delta\omega_c = \omega_c^{\text{output}} - \omega_c^{\text{input}}$ ) is the difference in the calculated  $t_c$  ( $\omega_c$ ) between the input and the output pulses.

of the Fourier transform of the time domain signal, and  $\omega$  is angular frequency. The deduced transmission times and center frequencies are shown in Fig. 3 as vertical lines, demonstrating a negative real time delay of  $\Delta t_c = -22.25$  ns and negative center frequency shift of  $\Delta\omega_c = -0.029$  Rad/ $\mu$ s.

**Discussion.** A full comparison of the time domain Gaussian pulse measurements with the predictions is summarized in Fig. 4. The data collected is over 4.9 GHz to 6.05 GHz, including four Feshbach modes [40, 78, 79], with 480 data points in total taken over the entire frequency range.

We see from Fig. 4, that the measured time-shifts  $\Delta t_c$  obtained with the Gaussian pulses, as well as the measured center-frequency shift  $\Delta\omega_c$ , are in excellent agreement with the  $D_t$  and  $D_\omega$  predictions of Asano, *et al* (Eqs. 2 and 3) [67]. These results are also reproduced by simulations of the ring graph (see Section I of [64]). Note the difference in scales for the frequency shifts in Figs. 4 (c) and (d), which shows that the frequency shift of the time-domain pulses increases with the predicted  $\tilde{\Delta}^2$  scaling. In all cases there are systematic deviations between the time-domain results and the predicted values from frequency domain complex time delay in the range between the Feshbach modes. These deviations are attributed to standing waves on the input and output coaxial cables used in the time-domain measurements, but calibrated out in the frequency domain measurements

(see Ref. [64] sections I, II, and VI for more details). We also note that the qualitative behavior of the center frequency shift shown in Fig. 4 (c-d) was predicted in Ref. [65].

In Ref. [67] there are also predictions made about the maximum time and frequency shifts that can be created by a given scattering system. The bounds represent the amplification of time delay (center frequency shift) from the scale of the inverse mode linewidth (mode linewidth) to that of the pulse duration (bandwidth). This amplification is analogous to that experienced for expectation values in quantum weak measurement [67] and superoscillatory functions [84, 85]. The bounds on time and frequency shifts are given by,  $D_{t,\text{max}} = \pm \frac{1}{\sqrt{2}\tilde{\Delta}}$  and  $D_{\omega,\text{max}} = \pm \frac{\tilde{\Delta}}{\sqrt{2}}$  respectively. In our case, for the pulses with a 1 MHz bandwidth, this would result in  $D_{t,\text{max}} \approx 265$  ns and  $D_{\omega,\text{max}} \approx 12$  Rad/ $\mu$ s, while for the 5 MHz bandwidth pulse case one has  $D_{t,\text{max}} \approx 53$  ns and  $D_{\omega,\text{max}} \approx 59$  Rad/ $\mu$ s. Our data for both of these cases, presented in Fig. 4 (as well as Fig. 5 in Section IV of Ref. [64]), are clearly well within these bounds. Our ring-graph measurement is in the strong-coupling limit, leading to reduced values of time-delay amplification [67].

One interesting observation is that the imaginary part of complex time delay produces changes in the carrier frequency so as to decrease the amount of absorption of the transmitted pulse [65, 83]. Related to this, Ref. [77] show a clear deviation from exponential decrease of laser



intensity with propagation distance in a dispersive absorbing medium, showing that the light is less attenuated at greater distances than one would expect. In the case of a scattering system with gain, it has also been noted that the center frequency shift will be towards (rather than away from) the gain mode [65, 83].

Our work generalizes that of Asano, *et al.* [67] in the sense that our predictions for  $D_t$  and  $D_\omega$  are not tied to any particular model of transmission near a resonant mode. We have shown that complex time delay derived from frequency-domain data provides model-free predictions for the pulse modifications due to scattering. This includes frequencies that are far from resonant modes, where the analytical approximations are no longer valid.

**Conclusions.** In this paper we experimentally demonstrate the connection between the real and imaginary components of transmission time delay and Gaussian pulse properties; verifying the predictions first laid out in Ref. [67]. The most novel contribution is the direct connection between the imaginary component of the

transmission time delay and the center frequency shift of the scattered Gaussian pulse. This helps bring physical meaning to an abstract but practically useful quantity making up the complex time delay.

In terms of future work, it would be interesting to generalize  $D_\omega$  and  $D_t$  to arbitrary pulse shapes. We can now make predictions for reflection time delays, along with reflection time-delay differences [37, 38], as well as transmission time-delay differences in non-reciprocal scattering systems [86]. The connection of this work to extreme time delays associated with scattering singularities [86, 87] is also of interest.

## ACKNOWLEDGMENTS

We thank Nadav Shaibe for helpful discussions. This work was supported by NSF/RINGS under grant No. ECCS-2148318, ONR under grant N000142312507, and DARPA/WARDEN under grant HR00112120021.

- 
- [1] J. Verbaarschot, H. Weidenmüller, and M. Zirnbauer, Grassmann integration in stochastic quantum physics: The case of compound-nucleus scattering, *Physics Reports* **129**, 367 (1985).
  - [2] V. V. Sokolov and V. Zelevinsky, Dynamics and Statistics of Unstable Quantum States, *Nucl.Phys.A* **504**, 562 (1989).
  - [3] H. Schomerus, Random matrix approaches to open quantum systems, in *Stochastic Processes and Random Matrices*, Lecture Notes of the Les Houches Summer School 2015, edited by G. Schehr, A. Altland, Y. V. Fyodorov, N. O’Connell, and L. F. Cugliandolo (Oxford University Press, 2017) pp. 409–473.
  - [4] A. Nock, S. Kumar, H. J. Sommers, and T. Guhr, Distributions of off-diagonal scattering matrix elements: Exact results, *Annals Phys.* **342**, 103 (2014).
  - [5] G. E. Mitchell, A. Richter, and H. A. Weidenmüller, Random matrices and chaos in nuclear physics: Nuclear reactions, *Reviews of Modern Physics* **82**, 2845 (2010).
  - [6] P. A. Mello, P. Pereyra, and T. H. Seligman, Information theory and statistical nuclear reactions. I. General theory and applications to few-channel problems, *Ann. Phys.* **161**, 10.1016/0003-4916(85)90080-6 (1985).
  - [7] Y. V. Fyodorov and H.-J. Sommers, Statistics of resonance poles, phase shifts and time delays in quantum chaotic scattering: Random matrix approach for systems with broken time-reversal invariance, *Journal of Mathematical Physics* **38**, 1918 (1997).
  - [8] Y. V. Fyodorov, D. V. Savin, and H.-J. Sommers, Scattering, reflection and impedance of waves in chaotic and disordered systems with absorption, *Journal of Physics A: Mathematical and General* **38**, 10731 (2005).
  - [9] Y. Fyodorov and D. Savin, Resonance scattering of waves in chaotic systems, in *The Oxford Handbook of Random Matrix Theory* (Oxford University Press, 2015).
  - [10] E. Doron, U. Smilansky, and A. Frenkel, Experimental demonstration of chaotic scattering of microwaves, *Physical Review Letters* **65**, 3072 (1990).
  - [11] A. Richter, Wave dynamical chaos: An experimental approach in billiards, *Physica Scripta* **2001**, 212 (2001).
  - [12] U. Kuhl, O. Legrand, and F. Mortessagne, Microwave experiments using open chaotic cavities in the realm of the effective Hamiltonian formalism, *Fortschritte der Physik* **61**, 404 (2013).
  - [13] O. Hul, M. Lawniczak, S. Bauch, A. Sawicki, M. Kuś, and L. Sirko, Are Scattering Properties of Graphs Uniquely Connected to Their Shapes?, *Physical Review Letters* **109**, 040402 (2012).
  - [14] G. Gradoni, J.-H. Yeh, B. Xiao, T. M. Antonsen, S. M. Anlage, and E. Ott, Predicting the statistics of wave transport through chaotic cavities by the random coupling model: A review and recent progress, *Wave Motion* **51**, 606 (2014).
  - [15] B. Dietz and A. Richter, Quantum and wave dynamical chaos in superconducting microwave billiards, *Chaos: An Interdisciplinary Journal of Nonlinear Science* **25**, 097601 (2015).
  - [16] U. Kuhl, H.-J. Stöckmann, and R. Weaver, Classical wave experiments on chaotic scattering, *Journal of Physics A: Mathematical and General* **38**, 10433 (2005).
  - [17] A. Bereczuk, B. Dietz, J. Che, J. Kuipers, J.-D. Urbina, and K. Richter, Universal S-matrix correlations for complex scattering of wave packets in noninteracting many-body systems: Theory, simulation, and experiment, *Physical Review E* **103**, 052209 (2021).
  - [18] D. Agassi, H. A. Weidenmüller, and G. Mantzouranis, The statistical theory of nuclear reactions for strongly overlapping resonances as a theory of transport phenomena, *Physics Reports* **22**, 145 (1975).
  - [19] L. Gao, L. Sun, F. Li, Q. Zhang, Y. Wang, T. Yu, J. Guo, Y. Bian, C. Li, X. Zhang, H. Li, J. Meng, and Y. He, 8-GHz Narrowband High-Temperature Superconducting Filter With High Selectivity and Flat Group Delay, *IEEE Transactions on Microwave Theory and Techniques* **57**,

- 1767 (2009).
- [20] H. A. Weidenmüller, Stochastic scattering theory random-matrix models for fluctuations in microscopic and mesoscopic systems, in *Chaos and Quantum Chaos*, edited by W. D. Heiss (Springer, 1992) pp. 121–166.
- [21] D. Trabert, S. Brennecke, K. Fehre, N. Anders, A. Geyer, S. Grundmann, M. S. Schöffler, L. P. H. Schmidt, T. Jahnke, R. Dörner, M. Kunitski, and S. Eckart, Angular dependence of the Wigner time delay upon tunnel ionization of H<sub>2</sub>, *Nature Communications* **12**, 1697 (2021).
- [22] C.-H. Zhang and U. Thumm, Streaking and Wigner time delays in photoemission from atoms and surfaces, *Physical Review A* **84**, 033401 (2011).
- [23] J. Kuipers, D. V. Savin, and M. Sieber, Efficient semiclassical approach for time delays, *New Journal of Physics* **16**, 123018 (2014).
- [24] M. Davy, Z. Shi, J. Wang, X. Cheng, and A. Z. Genack, Transmission Eigenchannels and the Densities of States of Random Media, *Physical Review Letters* **114**, 033901 (2015).
- [25] J. Carpenter, B. J. Eggleton, and J. Schröder, Observation of Eisenbud–Wigner–Smith states as principal modes in multimode fibre, *Nature Photonics* **9**, 751 (2015).
- [26] W. Xiong, P. Ambichl, Y. Bromberg, B. Redding, S. Rotter, and H. Cao, Spatiotemporal Control of Light Transmission through a Multimode Fiber with Strong Mode Coupling, *Physical Review Letters* **117**, 053901 (2016).
- [27] J. Böhm, A. Brandstötter, P. Ambichl, S. Rotter, and U. Kuhl, In situ realization of particlelike scattering states in a microwave cavity, *Physical Review A* **97**, 021801 (2018).
- [28] B. Gérardin, J. Laurent, P. Ambichl, C. Prada, S. Rotter, and A. Aubry, Particlelike wave packets in complex scattering systems, *Physical Review B* **94**, 014209 (2016).
- [29] A. Brandstötter, A. Girschik, P. Ambichl, and S. Rotter, Shaping the branched flow of light through disordered media, *Proceedings of the National Academy of Sciences* **116**, 13260 (2019).
- [30] M. Durand, S. M. Popoff, R. Carminati, and A. Goetschy, Optimizing Light Storage in Scattering Media with the Dwell-Time Operator, *Physical Review Letters* **123**, 243901 (2019).
- [31] U. R. Patel, Y. Mao, and E. Michielssen, Wigner–Smith time delay matrix for acoustic scattering: Theory and phenomenology, *The Journal of the Acoustical Society of America* **153**, 2769 (2023).
- [32] S. Fan and J. M. Kahn, Principal modes in multimode waveguides, *Optics Letters* **30**, 135 (2005).
- [33] U. R. Patel and E. Michielssen, Wigner–Smith Time-Delay Matrix for Electromagnetics: Theory and Phenomenology, *IEEE Transactions on Antennas and Propagation* **69**, 902 (2021).
- [34] Y. Mao, U. R. Patel, and E. Michielssen, Wigner–Smith Time Delay Matrix for Electromagnetics: Systems With Material Dispersion and Losses, *IEEE Transactions on Antennas and Propagation* **71**, 5266 (2023).
- [35] P. Ambichl, A. Brandstötter, J. Böhm, M. Kühmayer, U. Kuhl, and S. Rotter, Focusing inside Disordered Media with the Generalized Wigner-Smith Operator, *Physical Review Letters* **119**, 033903 (2017).
- [36] Y. V. Fyodorov, S. Suwunnarat, and T. Kottos, Distribution of zeros of the S-matrix of chaotic cavities with localized losses and coherent perfect absorption: Non-perturbative results, *Journal of Physics A: Mathematical and Theoretical* **50**, 30LT01 (2017).
- [37] Y. Fyodorov, Reflection Time Difference as a Probe of S-Matrix Zeros in Chaotic Resonance Scattering, *Acta Physica Polonica A* **136**, 785 (2019).
- [38] M. Osman and Y. V. Fyodorov, Chaotic scattering with localized losses: S-matrix zeros and reflection time difference for systems with broken time-reversal invariance, *Physical Review E* **102**, 012202 (2020).
- [39] L. Chen, S. M. Anlage, and Y. V. Fyodorov, Generalization of Wigner time delay to subunitary scattering systems, *Physical Review E* **103**, L050203 (2021).
- [40] L. Chen and S. M. Anlage, Use of transmission and reflection complex time delays to reveal scattering matrix poles and zeros: Example of the ring graph, *Physical Review E* **105**, 054210 (2022).
- [41] L. Eisenbud, *The formal properties of nuclear collisions*, Ph.D. thesis, Princeton University (1948).
- [42] E. P. Wigner, Lower Limit for the Energy Derivative of the Scattering Phase Shift, *Physical Review* **98**, 145 (1955).
- [43] F. T. Smith, Lifetime Matrix in Collision Theory, *Physical Review* **118**, 349 (1960).
- [44] Y. Huang, Y. Kang, and A. Z. Genack, Wave excitation and dynamics in non-Hermitian disordered systems, *Physical Review Research* **4**, 013102 (2022).
- [45] N. Lehmann, D. V. Savin, V. V. Sokolov, and H. J. Sommers, Time delay correlations in chaotic scattering: Random matrix approach, *Physica D: Nonlinear Phenomena* **86**, 572 (1995).
- [46] V. A. Gopar, P. A. Mello, and M. Büttiker, Mesoscopic capacitors: A statistical analysis, *Phys. Rev. Lett.* **77**, 3005 (1996).
- [47] T. S. Misirpashaev, P. W. Brouwer, and C. W. J. Beenakker, Spontaneous emission in chaotic cavities, *Phys. Rev. Lett.* **79**, 1841 (1997).
- [48] Y. V. Fyodorov, D. V. Savin, and H.-J. Sommers, Parametric correlations of phase shifts and statistics of time delays in quantum chaotic scattering: Crossover between unitary and orthogonal symmetries, *Phys. Rev. E* **55**, R4857 (1997).
- [49] Y. V. Fyodorov and Y. Alhassid, Photodissociation in quantum chaotic systems: Random-matrix theory of cross-section fluctuations, *Phys. Rev. A* **58**, R3375 (1998).
- [50] B. A. van Tiggelen, P. Sebbah, M. Stoytchev, and A. Z. Genack, Delay-time statistics for diffuse waves, *Phys. Rev. E* **59**, 7166 (1999).
- [51] P. W. Brouwer, K. M. Frahm, and C. W. J. Beenakker, Distribution of the quantum mechanical time-delay matrix for a chaotic cavity, *Waves in Random Media* **9**, 91 (1999).
- [52] D. V. Savin, Y. V. Fyodorov, and H.-J. Sommers, Reducing nonideal to ideal coupling in random matrix description of chaotic scattering: Application to the time-delay problem, *Phys. Rev. E* **63**, 035202 (2001).
- [53] T. Kottos and U. Smilansky, Quantum graphs: a simple model for chaotic scattering, *Journal of Physics A: Mathematical and General* **36**, 3501 (2003).
- [54] F. Mezzadri and N. J. Simm, Tau-function theory of chaotic quantum transport with  $\beta = 1, 2, 4$ , *Communications in Mathematical Physics* **324**, 465 (2013).
- [55] C. Texier and S. N. Majumdar, Wigner time-delay distri-

- bution in chaotic cavities and freezing transition, *Phys. Rev. Lett.* **110**, 250602 (2013).
- [56] M. Novaes, Statistics of time delay and scattering correlation functions in chaotic systems. I. Random matrix theory, *Journal of Mathematical Physics* **56**, 062110 (2015).
- [57] F. D. Cunden, Statistical distribution of the wigner-smith time-delay matrix moments for chaotic cavities, *Phys. Rev. E* **91**, 060102 (2015).
- [58] Y. Huang, C. Tian, V. A. Gopar, P. Fang, and A. Z. Genack, Invariance principle for wave propagation inside inhomogeneously disordered materials, *Phys. Rev. Lett.* **124**, 057401 (2020).
- [59] C. Texier, Wigner time delay and related concepts: Application to transport in coherent conductors, *Physica E: Low-dimensional Systems and Nanostructures Frontiers in Quantum Electronic Transport - In Memory of Markus Büttiker*, **82**, 16 (2016).
- [60] E. Pollak and W. H. Miller, New physical interpretation for time in scattering theory, *Physical Review Letters* **53**, 115 (1984).
- [61] R. Landauer and T. Martin, Barrier interaction time in tunneling, *Reviews of Modern Physics* **66**, 217 (1994).
- [62] H. G. Winful, Tunneling time, the Hartman effect, and superluminality: A proposed resolution of an old paradox, *Physics Reports* **436**, 1 (2006).
- [63] Y. Kang and A. Z. Genack, Transmission zeros with topological symmetry in complex systems, *Phys. Rev. B* **103**, L100201 (2021).
- [64] See supplemental material at [url will be inserted by publisher] for additional details., The Supplemental Material includes information on numerical simulations of the ring graph in the frequency- and time-domains, an examination of the extreme low transmission and large pulse bandwidth limits, additional analytical calculation details, plots of the experiment data over a wide frequency range, details on the time domain pulse measurements, details on potential sources of statistical and systematic error in the experiments, and further background information on complex time delay.
- [65] C. G. B. Garrett and D. E. McCumber, Propagation of a Gaussian Light Pulse through an Anomalous Dispersion Medium, *Physical Review A* **1**, 305 (1970).
- [66] S. Chu and S. Wong, Linear Pulse Propagation in an Absorbing Medium, *Physical Review Letters* **48**, 738 (1982).
- [67] M. Asano, K. Y. Bliokh, Y. P. Bliokh, A. G. Kofman, R. Ikuta, T. Yamamoto, Y. S. Kivshar, L. Yang, N. Imoto, Ş. K. Özdemir, and F. Nori, Anomalous time delays and quantum weak measurements in optical microresonators, *Nature Communications* **7**, 13488 (2016).
- [68] Ph. Balcou and L. Dutriaux, Dual Optical Tunneling Times in Frustrated Total Internal Reflection, *Physical Review Letters* **78**, 851 (1997).
- [69] H. Kogelnik and H. P. Weber, Rays, stored energy, and power flow in dielectric waveguides, *JOSA* **64**, 174 (1974).
- [70] Y. Aharonov, D. Z. Albert, and L. Vaidman, How the result of a measurement of a component of the spin of a spin-1/2 particle can turn out to be 100, *Physical Review Letters* **60**, 1351 (1988).
- [71] A. M. Steinberg, How Much Time Does a Tunneling Particle Spend in the Barrier Region?, *Physical Review Letters* **74**, 2405 (1995).
- [72] Y. Aharonov, N. Erez, and B. Reznik, Superluminal tunnelling times as weak values, *Journal of Modern Optics* **50**, 1139 (2003).
- [73] D. R. Solli, C. F. McCormick, R. Y. Chiao, S. Popescu, and J. M. Hickmann, Fast light, slow light, and phase singularities: A connection to generalized weak values, *Physical Review Letters* **92**, 043601 (2004).
- [74] N. Brunner, V. Scarani, M. Wegmüller, M. Legré, and N. Gisin, Direct Measurement of Superluminal Group Velocity and Signal Velocity in an Optical Fiber, *Physical Review Letters* **93**, 203902 (2004).
- [75] N. Brunner and C. Simon, Measuring Small Longitudinal Phase Shifts: Weak Measurements or Standard Interferometry?, *Physical Review Letters* **105**, 010405 (2010).
- [76] H. Cao, A. Dogariu, and L. Wang, Negative group delay and pulse compression in superluminal pulse propagation, *IEEE Journal of Selected Topics in Quantum Electronics* **9**, 52 (2003).
- [77] M. A. I. Talukder, Y. Amagishi, and M. Tomita, Superluminal to subluminal transition in the pulse propagation in a resonantly absorbing medium, *Physical Review Letters* **86**, 3546 (2001).
- [78] D. Waltner and U. Smilansky, Scattering from a ring graph - a simple model for the study of resonances, *Acta Physica Polonica A* **124**, 1087 (2013).
- [79] D. Waltner and U. Smilansky, Transmission through a noisy network, *Journal of Physics A: Mathematical and Theoretical* **47**, 355101 (2014).
- [80] M. Bialous, P. Dulian, A. Sawicki, and L. Sirko, Delay-time distribution in the scattering of short gaussian pulses in microwave networks, *Physical Review E* **104**, 024223 (2021).
- [81] A. Akhshani, M. Bialous, and L. Sirko, Quantum graphs and microwave networks as narrow-band filters for quantum and microwave devices, *Physical Review E* **108**, 034219 (2023).
- [82] P. Sebbah, O. Legrand, and A. Z. Genack, Fluctuations in photon local delay time and their relation to phase spectra in random media, *Physical Review E* **59**, 2406 (1999).
- [83] B. Macke and B. Ségard, Propagation of light-pulses at a negative group-velocity, *The European Physical Journal D - Atomic, Molecular, Optical and Plasma Physics* **23**, 125 (2003).
- [84] M. V. Berry and S. Popescu, Evolution of quantum superoscillations and optical superresolution without evanescent waves, *Journal of Physics A: Mathematical and General* **39**, 6965 (2006).
- [85] M. V. Berry, Optical currents, *Journal of Optics A: Pure and Applied Optics* **11**, 094001 (2009).
- [86] N. Shaibe, J. M. Erb, and S. M. Anlage, Superuniversal statistics of complex time-delays in non-hermitian scattering systems (2024), arXiv:2408.05343 [nlin.CD].
- [87] J. Erb, N. Shaibe, R. Calvo, D. Lathrop, T. Antonsen, T. Kottos, and S. M. Anlage, Novel topology and manipulation of scattering singularities in complex non-hermitian systems (2024), arXiv:2411.01069 [cond-mat.mes-hall].

# A Physical Interpretation of Imaginary Time Delay Supplementary Material

Isabella L. Giovannelli\* and Steven M. Anlage  
 Maryland Quantum Materials Center, Department of Physics  
 University of Maryland, College Park, Maryland 20742, USA  
 (Dated: December 18, 2024)

Here we discuss further details about numerical simulations of the ring graph in both the frequency-domain and time-domain (Section I), the renormalization of complex time delay for low-transmission (Section II), details of the transmitted pulse analytical calculation (Section III), plots of the data over the full measurement frequency range (Section IV), detailed discussion of the time-domain measurements (Section V), a discussion of both systematic and random errors in the experiment (Section VI), and further background information about complex time delay (Section VII).

## I. SIMULATION

The frequency-domain and time-domain simulations of the ring graph were performed using CST Studio Suite 2021. Fig. 1 shows the model used for the CST simulations.

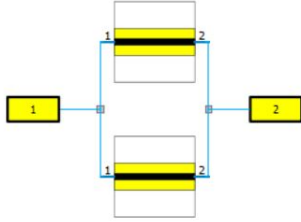


FIG. 1. CST model of microwave ring graph used for simulations consisting of two ports, two T-junctions (small gray squares), and two coaxial cables (large gray squares). The coaxial cables are identical except for their lengths which differ by 1 inch. The blue lines are zero-length electrical connections.

This model consists of two ports, two T-junctions, and two coaxial cables. The diameters of the inner and outer conductors for the coaxial cables are 0.091 cm and 0.298 cm respectively. The other parameters set for the coaxial cables include the relative permittivity ( $\epsilon_r$ ) which is 2.01047, the dielectric loss tangent which is  $\tan \delta = 0.00028$ , and the metal resistivity normalized to gold resistivity which is 1.8. The upper coaxial cable in Fig. 1 has a length of 11 in (27.9 cm) and the lower coaxial cable has a length of 12 in (30.5 cm).

The ring graph is interesting because it supports two types of modes [1, 2]. One set have standing wave maxima near the leads, establishing strong coupling to the leads, and creating low-Q resonances known as shape resonances. The other modes are standing wave patterns rotated by 90-degrees in phase compared to the shape modes, leading to smaller coupling to the leads and high-Q resonances, and are known as Feshbach resonances. The features arising from each of these two classes of resonances are evident in the  $S_{21}(f)$  data shown in Figs. 2(a) and 4(a) below.

Figure 2 contains a summary of our main simulated results. Fig. 2(a) are the four scattering parameters of the 2-port device as a function of frequency, which we note are very similar in character to those for the measured ring graph shown in Fig. 4(a) below. Note that these results are obtained using the frequency domain “S-parameters” task in CST. The complex transmission time delay is calculated from  $S_{21}(f)$ . In Fig. 2(b), the predicted pulse center frequency shift  $D_\omega$  for a 5 MHz bandwidth pulse is plotted, which is calculated using the imaginary part of the transmission time delay, see Eqs. 5 and 19 of the main text. The shift in center frequency of the simulated Gaussian time-domain pulse ( $\Delta\omega_c$ ) is plotted on top as red diamonds. This is done over the center-frequency range of 0.377 GHz to 1.2 GHz for a 5 MHz bandwidth Gaussian pulse. Note that the Gaussian pulse simulations are done using the time domain “transient” task in CST where the input excitations (i.e. Gaussian pulses) are generated in Matlab using the same equation used in the experiment (see Eq.14).

Fig. 2(c) shows the time shift predictions, analogous to Fig. 2(b), as a function of pulse center-frequency. The real part of the transmission time delay  $D_t$  is obtained directly from the frequency domain simulation of  $S_{21}(f)$ . The shift in transmission time of the simulated time-domain Gaussian pulse ( $\Delta t_c$ ) is plotted on top as red diamonds. This is done over the same center-frequency range of 0.377 GHz to 1.2 GHz for a 5 MHz bandwidth Gaussian pulse. The agreement between the two methods of calculating center frequency shift and time delay agree to the same extent as in the experiment.

## II. EXTREME LOW TRANSMISSION AND LARGE PULSE BANDWIDTH LIMITS

It was noted in Eq. 11 of Ref. [3] that in the extreme low transmission limit one must adjust the predictions for

\* igiovann@umd.edu



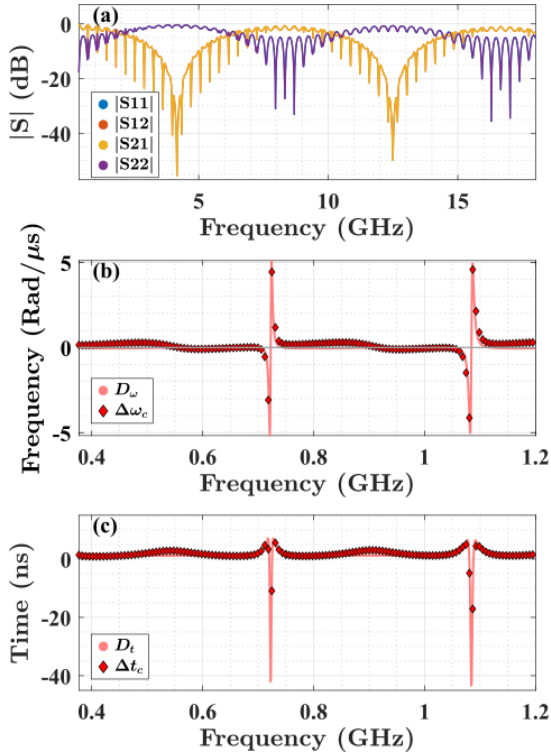


FIG. 2. (a) Simulated scattering parameters for the ring graph model depicted in Fig. 1. (b) Simulation results for the frequency shift of the Gaussian pulse with a bandwidth of 5 MHz. (c) Corresponding simulation results for the time shift of a Gaussian pulse with a bandwidth 5 MHz.

shifts in time and frequency ( $D_t$  and  $D_\omega$ ) that the Gaussian pulse experiences when the time delay diverges. For convenience, these equations for  $D'_t$  and  $D'_\omega$  are reproduced below in the notation used in this paper,

$$D'_t = \frac{\text{Re}[\tau_T(\omega_c; \alpha)]}{1 + \frac{\tilde{\Delta}^2 |\tau_T(\omega_c; \alpha)|^2}{2}} \quad D'_\omega = \frac{-\tilde{\Delta}^2 \text{Im}[\tau_T(\omega_c; \alpha)]}{1 + \frac{\tilde{\Delta}^2 |\tau_T(\omega_c; \alpha)|^2}{2}} \quad (1)$$

where again  $\tau_T(\omega_c; \alpha)$  is the transmission time delay defined in equation 5 of the main text and  $\tilde{\Delta}$  is the pulse bandwidth defined in equation 8 of the main text, and  $\alpha$  is the system's uniform loss. The addition of a renormalization term in the denominators of Eq. 1 prevents divergence of the predicted time delay and frequency shift.

In Figure 3 we show a summary of results in the limits of low transmission and large pulse bandwidths. These measurements were performed over the mode with the lowest level of transmission in our system, which is in the frequency range 4.15 GHz to 4.63 GHz. To see how the transmission at this mode compares with others in the system, please see Fig. 4(a) for a plot of the scattering parameters over the frequency range 0.377 GHz to 18 GHz.

For the small pulse bandwidth case of 5 MHz (Fig. 3(a) and (c)) we see that low-transmission predictions  $D'_t$  and

$D'_\omega$  are both smaller in amplitude than the original  $D_t$  and  $D_\omega$  predictions. Here we see that the time domain experiment results seem to better follow the corrected low-transmission predictions in that the peaks are less extreme. Note that in this region the transmission is quite low ( $< -40$  dB) and the modes in the 4.4 GHz - 4.55 GHz region are non-trivial and overlapping (as seen in the associated scattering parameters plotted in Fig. 3(a)). This made this case particularly difficult to examine experimentally and is why there is a substantial amount of noise present.

We do not see much difference between  $D'_t$ ,  $D'_\omega$  and  $D_t$ ,  $D_\omega$  until a Gaussian pulse with a large bandwidth is considered. These results are shown in Fig. 3(b) and (d) for a pulse with a bandwidth of 100 MHz. Here we see an extreme decrease in the amplitude of the predictions for  $D'_t$  and  $D'_\omega$  relative to  $D_t$  and  $D_\omega$ . The time domain experimental data (in green) clearly follows the corrected low-transmission predictions  $D'_t$  and  $D'_\omega$  more closely than the  $D_t$  and  $D_\omega$  predictions.

Overall, we see that the renormalized predictions for frequency and time shifts in low-transmission regions are generally valid. Particularly for the case where the pulse bandwidth is large in comparison to the 3 dB bandwidth of the chosen resonance. For the small bandwidth case, the experimental results are still consistent with the predictions, but the difference that the correction makes is significantly smaller than for the large bandwidth case.

### III. TRANSMITTED PULSE CALCULATION DETAILS

In this section we reproduce the derivation linking transmission time delay to the characteristics of a Gaussian pulse. This is done by combining methods used in Asano *et al.* [3] and Cao *et al.* [4]. The assumptions underlying this calculation include the following. i) The frequency bandwidth of the pulse  $\tilde{\Delta}$  is much smaller than the carrier frequency of the wave  $\omega_c$ , as well as the 3-dB linewidth of the resonant mode being studied  $\gamma_{3\text{-dB}}$ , ii) the propagation distance  $z$  through the system satisfies  $z \ll z_\alpha (\gamma_{3\text{-dB}}/\tilde{\Delta})^2$ , [5] where  $z_\alpha$  is the absorption length of the medium.

The frequency domain equation for the input Gaussian pulse is given by:

$$E_i(\omega) = \frac{B}{\tilde{\Delta}} \exp \left[ -\frac{(\omega - \omega_c)^2}{2\tilde{\Delta}^2} \right] \quad (2)$$

where  $\omega_c$  is the carrier angular frequency,  $B$  is the initial amplitude, and

$$\tilde{\Delta} = \frac{\pi \tilde{\Delta}_\omega}{\sqrt{2 \ln 2}} \quad (3)$$

where  $\tilde{\Delta}_\omega$  is the desired angular frequency bandwidth of the pulse. Note that  $\tilde{\Delta}_\omega$  is equal to the full width at

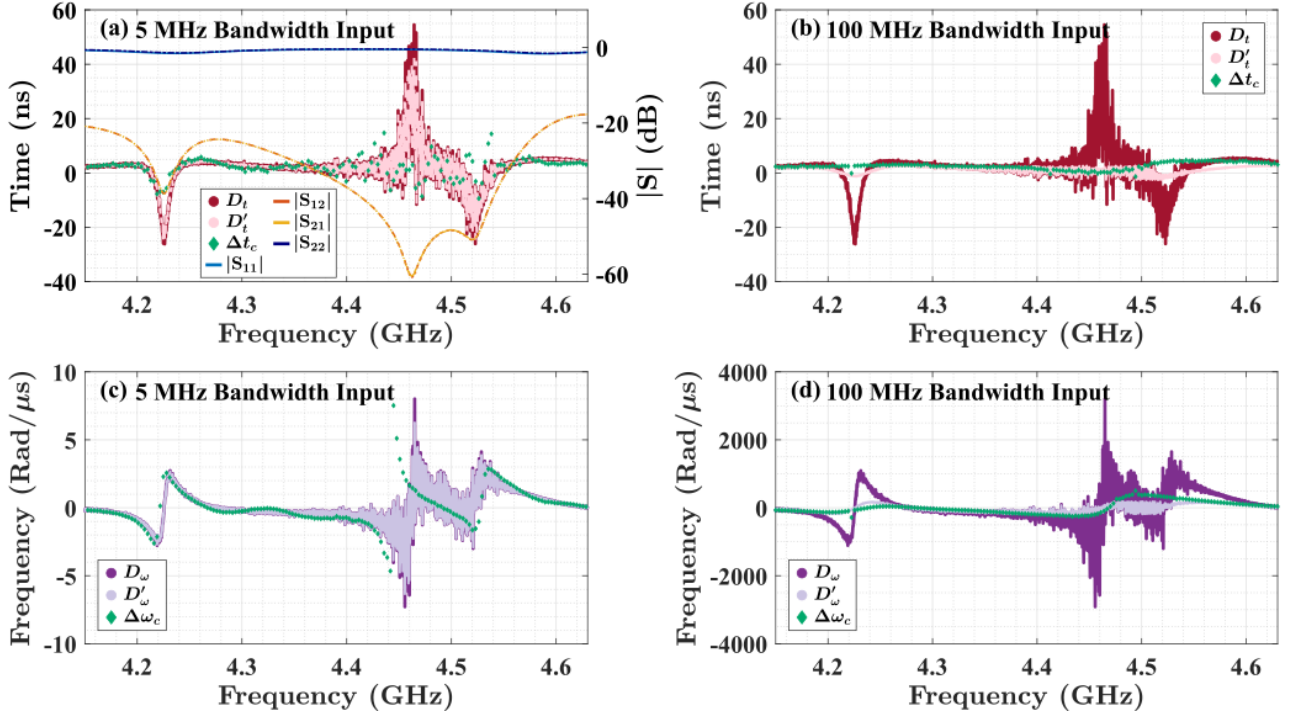


FIG. 3. Summary of low transmission and large pulse bandwidth results. (a) This plot is for the case where the frequency bandwidth of the input pulse is 5 MHz. The left axis is plotting the shift in time predicted using the original form of  $D_t$  in dark red and the adjusted form of  $D'_t$  for extreme low transmission in pink. The shift in transmission time of the Gaussian pulses is shown as green diamonds. The right axis is in dB and corresponds to the scattering parameters listed in the legend. Note that these scattering parameters are the same for every plot in this figure. (b) Same as (a) except this plot is for the case where the frequency bandwidth of the input pulse is 100 MHz. (c-d) These are the corresponding plots for the shift in frequency case. In dark purple is the original shift in frequency prediction  $D_\omega$  (see eqn. 21 in the main text). On top in light purple is the form of  $D'_\omega$  that is for the case of extreme low transmission. The green diamonds are the measured shift in frequency of the Gaussian pulses sent through our experiment.

half maximum (FWHM) of the Gaussian curve in the frequency domain space.

The frequency domain equation for the output Gaussian pulse is given by:

$$E_o(\omega; \alpha) = T(\omega + i\alpha)E_i(\omega) \quad (4)$$

where  $T(\omega + i\alpha)$  is the transmission coefficient of the lossy scattering system, and  $\alpha$  quantifies the uniform loss. Following the transcription in [4], we define

$$A(\omega; \alpha) = \frac{1}{|T(\omega + i\alpha)|} \quad (5)$$

which quantifies both absorption (when  $|T(\omega + i\alpha)| < 1$ ) and gain (when  $|T(\omega + i\alpha)| > 1$ ). We then define the real “transfer coefficient” to be  $\kappa(\omega; \alpha) = \ln(A(\omega; \alpha))$ . Putting this together we get,

$$E_o(\omega; \alpha) = \exp[-\kappa(\omega; \alpha) + i\phi(\omega; \alpha)] E_i(\omega) \quad (6)$$

where  $\phi$  is the phase of the transmission coefficient.

We now require that the bandwidth of this Gaussian pulse to be narrow such that  $|T(\omega; \alpha)|$  and  $\phi(\omega; \alpha)$  only experience slight variation over the bandwidth of the

pulse. This then allows us to expand  $\kappa(\omega; \alpha)$  and  $\phi(\omega; \alpha)$  into a Taylor series, centered around the carrier frequency  $\omega_c$

$$\kappa(\omega; \alpha) = \kappa(\omega_c; \alpha) + \left. \frac{d\kappa(\omega; \alpha)}{d\omega} \right|_{\omega_c} (\omega - \omega_c) + \dots \quad (7)$$

$$\phi(\omega; \alpha) = \phi(\omega_c; \alpha) + \left. \frac{d\phi(\omega; \alpha)}{d\omega} \right|_{\omega_c} (\omega - \omega_c) + \dots \quad (8)$$

in this case we assume the bandwidth is sufficiently narrow such that higher order terms can be neglected. These expansions can then be related to the real and imaginary parts of the transmission time delay. Calculating the transmission time delay associated with the generalized transmission coefficient  $T(\omega + i\alpha) = \exp[-\kappa(\omega; \alpha) + i\phi(\omega; \alpha)]$  yields,

$$\tau_T(\omega; \alpha) = -i \frac{\partial}{\partial \omega} \ln [\exp[-\kappa(\omega; \alpha) + i\phi(\omega; \alpha)]] \quad (9)$$

$$= \frac{\partial \phi(\omega; \alpha)}{\partial \omega} + i \frac{\partial \kappa(\omega; \alpha)}{\partial \omega} \quad (10)$$

$$= \text{Re}[\tau_T] + i \text{Im}[\tau_T] \quad (11)$$

Combining equations 7 and 8 with 10 and 11 results in

the following expressions for  $\kappa$  and  $\phi$ ,

$$\kappa(\omega; \alpha) \approx \kappa(\omega_c; \alpha) + \text{Im}[\tau_T(\omega_c; \alpha)](\omega - \omega_c) \quad (12)$$

$$\phi(\omega; \alpha) \approx \phi(\omega_c; \alpha) + \text{Re}[\tau_T(\omega_c; \alpha)](\omega - \omega_c) \quad (13)$$

Putting these results (lines 12 and 13) into equation 6 results in the following,

$$\begin{aligned} E_o(\omega; \alpha) &= E_i(\omega) \times \exp[-(\kappa(\omega_c; \alpha) + \text{Im}[\tau_T(\omega_c; \alpha)](\omega - \omega_c))] \times \exp[i(\phi(\omega_c; \alpha) + \text{Re}[\tau_T(\omega_c; \alpha)](\omega - \omega_c))] \\ &= E_i(\omega)T(\omega_c + i\alpha) \times \exp[-\text{Im}[\tau_T(\omega_c; \alpha)] + i\text{Re}[\tau_T(\omega_c; \alpha)](\omega - \omega_c)] \end{aligned}$$

Now we add in the expression for the Gaussian pulse for the input wave (main text equation 7).

$$= \frac{B}{\tilde{\Delta}} T(\omega_c + i\alpha) \times \exp\left[-\frac{(\omega - \omega_c)^2}{2\tilde{\Delta}^2} - \text{Im}[\tau_t(\omega_c; \alpha)](\omega - \omega_c)\right] \times \exp[i\text{Re}[\tau_T(\omega_c; \alpha)](\omega - \omega_c)]$$

Next we complete the square in the argument of the exponential.

$$\begin{aligned} &= \frac{B}{\tilde{\Delta}} T(\omega_c + i\alpha) \times \exp\left[\frac{-\left((\omega - \omega_c) + \tilde{\Delta}^2 \text{Im}[\tau_T(\omega_c; \alpha)]\right)^2}{2\tilde{\Delta}^2} + \frac{1}{2}\tilde{\Delta}^2 \text{Im}[\tau_t(\omega_c; \alpha)]^2\right] \times \exp[i\text{Re}[\tau_T(\omega_c; \alpha)](\omega - \omega_c)] \\ &= \frac{B}{\tilde{\Delta}} T(\omega_c + i\alpha)C_o(\omega_c; \alpha) \times \exp\left[\frac{-\left((\omega - \omega_c) - D_\omega\right)^2}{2\tilde{\Delta}^2}\right] \times \exp[iD_t(\omega - \omega_c)] \\ &= T(\omega_c + i\alpha)C_o(\omega_c; \alpha) \times E_i(\omega - D_\omega) \times \exp[iD_t(\omega - \omega_c)] \end{aligned}$$

where  $C_o(\omega_c; \alpha) = \exp\left[\frac{1}{2}\tilde{\Delta}^2 \text{Im}[\tau_T(\omega_c; \alpha)]^2\right]$  is constant at a specific center frequency  $\omega_c$  and loss parameter  $\alpha$ . From this final expression, we see that the output pulse is shifted in the frequency space by  $D_\omega = -\tilde{\Delta}^2 \text{Im}[\tau_T(\omega_c; \alpha)]$ , relating the shift to the imaginary part of the transmission time delay. In the time domain, one can show in an analogous fashion that the temporal shift of the pulse is  $D_t = \text{Re}[\tau_T(\omega_c; \alpha)]$ , which relates the time-shift of the pulse to the real part of the transmission time delay.

#### IV. PLOTS OF DATA OVER THE FULL FREQUENCY RANGE

In this section we show the measured S-parameters and complex time delay of the ring graph over the entire measured frequency range (0.377 - 18 GHz). Figure 4(a) shows the scattering parameters for the ring graph shown in Fig. 1 of the main text. These are measured using a calibrated network analyzer. See the main text ‘Experiment’ section for more details. Figure 4(b) shows the derived complex transmission time delay (in ns) as a function of frequency for the ring graph.

In this section we also have Gaussian pulse time and frequency shift results over the full frequency range from 0.377 GHz to 18 GHz. These results are shown in Fig. 5 where Fig. 5(a) illustrates the time shift results and Fig. 5(b) shows the analogous frequency shift results. The scattering parameters are reproduced on each plot to show the correspondence between the resonant modes and the experienced time/frequency shifts. In both cases we see that in general we have excellent agreement be-

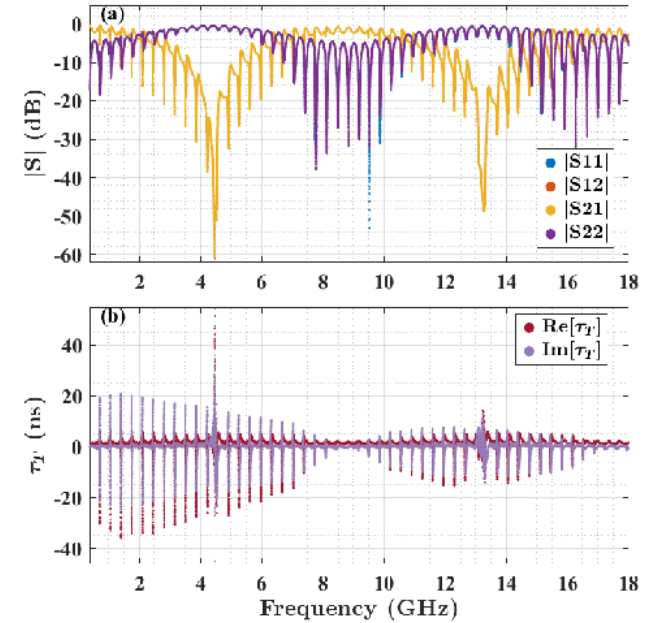


FIG. 4. (a) Full S-parameter data for the microwave ring graph collected over the frequency range 0.377 GHz to 18 GHz. (b) The corresponding calculated transmission time delay  $\tau_T$  (in ns) with both its real and imaginary parts plotted.

tween  $D_t$  and  $\Delta t_c$ , and  $D_\omega$  and  $\Delta\omega_c$ . In other words, this data indicates that there is a strong connection between complex time delay and the center time and frequency shifts experienced by a Gaussian pulse as it travels through a ring-graph resonator. Specifically, this sup-

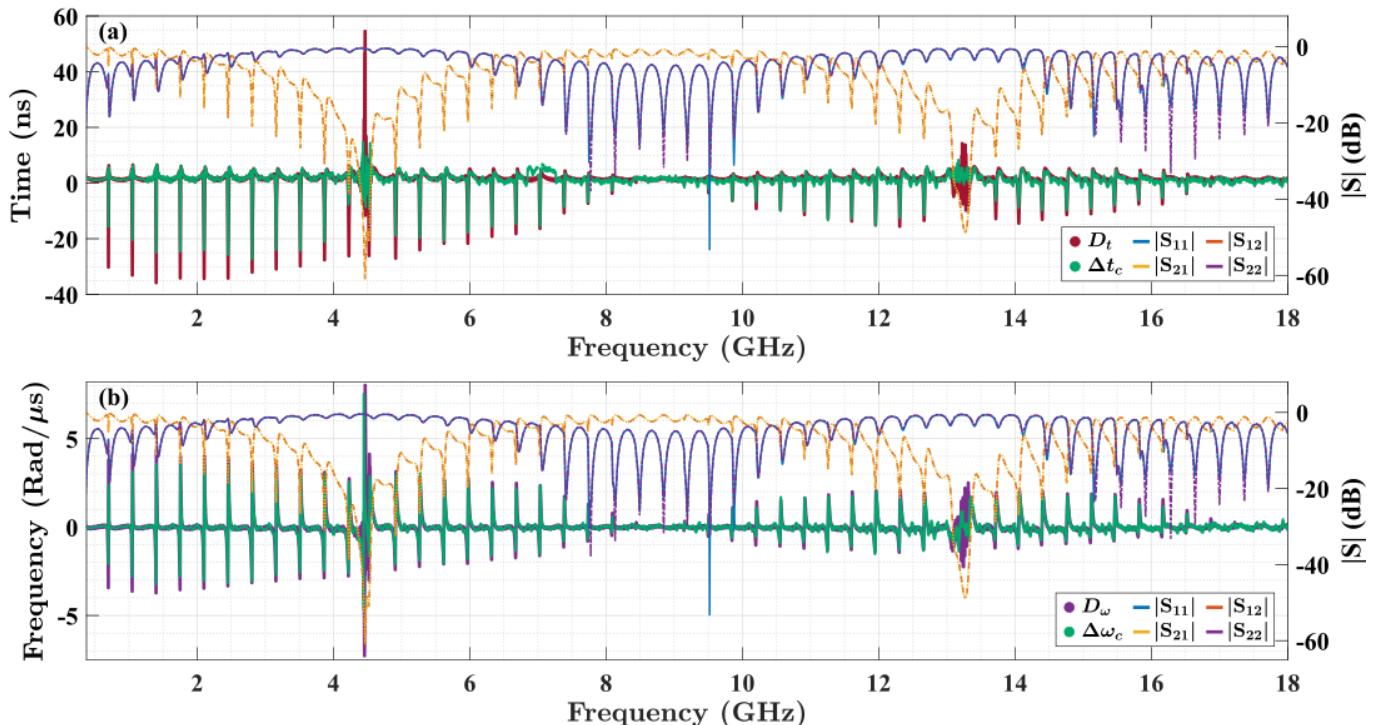


FIG. 5. Summary of the main results for the case where the input Gaussian pulse has a 5 MHz bandwidth. The data was collected over the frequency range 0.377 GHz to 18 GHz. (a) shows the time delays  $D_t$  and  $\Delta t_c$  as a function of frequency, and (b) shows the frequency shifts  $D_\omega$  and  $\Delta\omega_c$  as a function of frequency. In both parts the full set of scattering parameters are plotted using the right axis.

ports the conclusion that the real part of transmission time delay corresponds to a time shift in the Gaussian pulse and the imaginary part of transmission time delay is related to a center frequency shift in the Gaussian pulse.

In both Fig. 5(a) and Fig. 5(b) we see that as frequency increases, there is an increase in oscillatory behavior in the green time domain data ( $\Delta t_c$  and  $\Delta\omega_c$ ) in the regions in between the Feshbach modes. For example, in the region 0.377 GHz to 0.6 GHz, we see that the green time domain data is mostly flat and in agreement with the predictions  $D_t$  and  $D_\omega$ . However, in the region around 12 GHz to 12.25 GHz, we see that the green time domain data has picked up some oscillatory behavior that is not present in the  $D_t$  and  $D_\omega$  prediction curves. We believe that this is a result of a discrepancy between the system used for time domain measurements and the frequency domain setup. Please see section VI of the Supp. Mat. for more details.

## V. TIME DOMAIN PULSE MEASUREMENTS

In this section we go into more detail about how the Gaussian pulses are created in the experiment. We also discuss how time delay and center-frequency shift are measured in the time domain setup. Specifically here we discuss how the time delay arising from the input and

output cables (shown in Fig. 6(c)) is removed from the measurement to isolate the time delay just due to the graph.

The Gaussian pulses used in our experiment are created on the AWG using the equation,

$$E_i(t) = \cos(\omega_c(t - t_0)) \exp \left[ -\frac{(t - t_0)^2 \Delta^2}{\sqrt{2 \ln 2}} \right] \quad (14)$$

where  $\omega_c = 2\pi f_c$  and  $f_c$  is the selected center frequency of the Gaussian pulse. The variable  $t_0$  is where the pulse is centered in time in the AWG memory, and this is chosen to be 3000 ns for the 1 MHz bandwidth case and 5000 ns for the 5 MHz bandwidth case. These values are chosen so that the pulse is fully generated by the AWG. Note that this choice is mostly arbitrary and the exact number itself does not hold any physical significance. Lastly,

$$\Delta = \frac{\pi \Delta_f}{\sqrt{2 \ln 2}} \quad (15)$$

where  $\Delta_f$  is the FWHM of the Gaussian pulse in the linear frequency space.

In all of our measurements we are comparing the properties of a Gaussian pulse that has traveled through the ring graph (called the output pulse) to those of the original input Gaussian pulse. In both of these cases there is additional delay due to the cables in our time-domain system (external to the ring graph) that has to be removed.



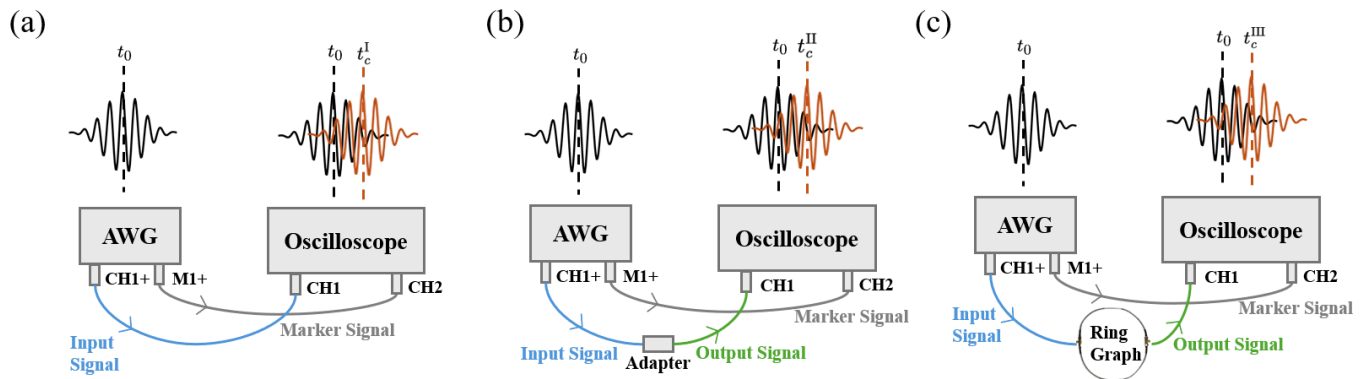


FIG. 6. Summary of the different time domain setups used to measure and remove the time delay associated with the input and output cables, and to determine the delay associated with just the ring graph. (a) Schematic of the time delay measurement to determine delay associated with the input cable (blue). (b) Schematic of the time delay measurement to determine delay associated with both the input cable and output cable (green) along with a Female-Female adapter. (c) Schematic of the time delay measurement to determine delay associated with the input cable, ring graph, and output cable.

See Fig. 6 for a visualization of these cases. Note that these additional cables do not play a role in the frequency domain measurements because they are calibrated out of the S-parameter measurement.

For the input pulse case, first the Gaussian pulse is created using the AWG and centered at a particular time  $t_0$  in the device memory. The pulse is output from the AWG and sent through the same cable that would normally be connected to the ring graph, except in this case the cable is connected directly to the oscilloscope where the input pulse (that will be delivered to the ring-graph) can then be measured, see Fig. 6(a). The transmission time  $t_c^I$  is calculated from the measured pulse in this case using the same formula defined in the main text in Eq. 4. We know that if there were no delay in the cable the measured transmission time of the pulse should be  $t_0$  in the oscilloscope memory, so we subtract out any additional delay added by the input cable ensuring the measured input pulse is centered at  $t_0$ . Thus,  $\Delta t_{delay}^{in} = t_c^I - t_0$  where we now define  $t_c^{input} = t_c^I - \Delta t_{delay}^{in} = t_0$ .

A similar process is performed for the output pulse case. For this case, the pulse first travels through the input cable, through the ring graph, and then through an output cable. See Fig. 6(c). To remove the time delay in the cables we perform a measurement where we remove the ring graph and replace it with an electrically short Female-to-Female (f2f) coaxial cable adapter, see Fig. 6(b). From here we repeat the same process as for the input pulse case. We subtract any delay ensuring that the output pulse is centered at  $t_0$  in the oscilloscope memory. The additional delay from the f2f adapter is taken into account by measuring its electrical length using a microwave vector network analyzer and then estimating its delay. The estimated delay for this f2f adapter is approximately  $t_{delay}^{adapter} = 0.014$  ns. The total delay for this case is calculated as  $\Delta t_{delay}^{out} = t_c^{II} - t_0 - t_{delay}^{adapter}$  where  $t_c^{II}$  is the time depicted in Fig. 6(b) and is calcu-

lated using Eq. 4 in the main text. Finally we calculate  $t_c^{output} = t_c^{III} - \Delta t_{delay}^{out}$  for the final transmission time value with the delay arising from the cables removed. The time  $t_c^{III}$  is the transmission time measured in the setup of Fig. 6(c). Note that the  $\Delta t_c$  values shown in the main text are then calculated as  $\Delta t_c = t_c^{output} - t_c^{input}$ .

Lastly, note that for the calculation of carrier frequency shift  $\Delta\omega_c$  there is no time delay subtraction since this calculation is done entirely in the frequency space where constant time shifts are not relevant.

## VI. SYSTEMATIC AND RANDOM ERRORS IN THE EXPERIMENT

The following sub-sections serve to explain and document the main known possible sources of error in our experiment.

### A. Time Domain Equipment limitations

The time domain experiment requires coordinated measurements with an Arbitrary Waveform Generator (AWG) and an oscilloscope (DSO). The details of the AWG and DSO models used in the experiments are given in the ‘Transmission Time Delay Measurements’ section of the main text.

For the AWG we expect the error in pulse center frequency to be at most  $\pm 50$  kHz ( $\pm 0.31$  Rad/ $\mu$ s). This number is estimated based on the age of the internal reference clock of the AWG. The trigger jitter in the DSO is 116 fs (rms).

To better assess how the limitations of the equipment impacts the experimental data, specifically the center-frequency data, we performed a variety of fidelity measurements. One motivation to examine the accuracy of the center-frequency data was because of the visible noise

present in Fig. 4(c) of the main text. The setup for these measurements is depicted in Fig. 6(a) where we have a single cable connecting the AWG and DSO. A pulse is created in the AWG and sent to the DSO, which performs a triggered measurement of the pulse. The DSO then performs an averaged measurement over 16 realizations. The final average is considered a single measurement. This process is then repeated 1000 times for various choices of pulse bandwidths. We then take this time domain data, Fourier Transform it using Matlab, and measure the center frequency of the transmitted pulse. The center frequency is calculated using Eq. 5 of the main text. This value is then compared with the specified center frequency of the original input pulse. The difference between the input and output center-frequencies will be referred to as  $\Delta\omega_c = \omega_c^{\text{output}} - \omega_c^{\text{input}}$ . In this scenario, where the pulse is traveling through a single simple coaxial cable, we expect  $|\Delta\omega_c| \approx 0$ .

A summary of these results are shown in Fig. 7 for the cases of an input Gaussian pulse with bandwidths of 1 MHz, 5 MHz, and 100 MHz, all centered at 5.23 GHz. For the 1 MHz case, Fig. 7(a), the mean of the data collected is  $-0.006 \text{ Rad}/\mu\text{s}$  with a variance of  $0.005 \text{ Rad}/\mu\text{s}$ . For the 5 MHz case, Fig. 7(b), the mean of the histogram is  $-0.005 \text{ Rad}/\mu\text{s}$  and the variance is  $0.011 \text{ Rad}/\mu\text{s}$ . Lastly, for the 100 MHz case, Fig. 7(c), the mean of the data is  $0.472 \text{ Rad}/\mu\text{s}$  and the variance is  $0.139 \text{ Rad}/\mu\text{s}$ . In an ideal scenario, we would expect to have a mean of 0 for all of these cases. In other words, there is no difference between the input Gaussian pulse center frequency and the output Gaussian pulse center frequency when the pulse travels through a single coaxial cable. We see that the means for the 1 MHz and the 5 MHz cases are virtually identical, while for the 100 MHz case the error is significantly larger.

At first glance it might seem that the larger error present in the 100 MHz bandwidth results is problematic, but when looking at the results shown in Fig. 3(d) we see that the frequency shifts are on the scale of  $10^3 \text{ Rad}/\mu\text{s}$ . Thus, an error of  $\pm 0.472 \text{ Rad}/\mu\text{s}$  is negligibly small in comparison. Similarly, if we look at the results for the 5 MHz bandwidth case shown in Fig. 3(c) we see that the frequency shifts are on the order of  $1 \text{ Rad}/\mu\text{s}$ . Again this is significantly larger than the measured error of  $\pm 0.005 \text{ Rad}/\mu\text{s}$ . For the 1 MHz bandwidth case, please refer to Fig. 4(c) of the main text. Here we see that the frequency shifts scale on the order of  $0.05\text{-}0.1 \text{ Rad}/\mu\text{s}$ . The error for this case was  $\pm 0.006 \text{ Rad}/\mu\text{s}$ . We see in Fig. 4(c) of the main text that the data is noisiest when the magnitude of the measured frequency shifts are roughly less than  $0.01 \text{ Rad}/\mu\text{s}$ . Thus, its likely that the ‘‘noise’’ we see in Fig. 4(c) is simply the result of us reaching the limits of our equipment.

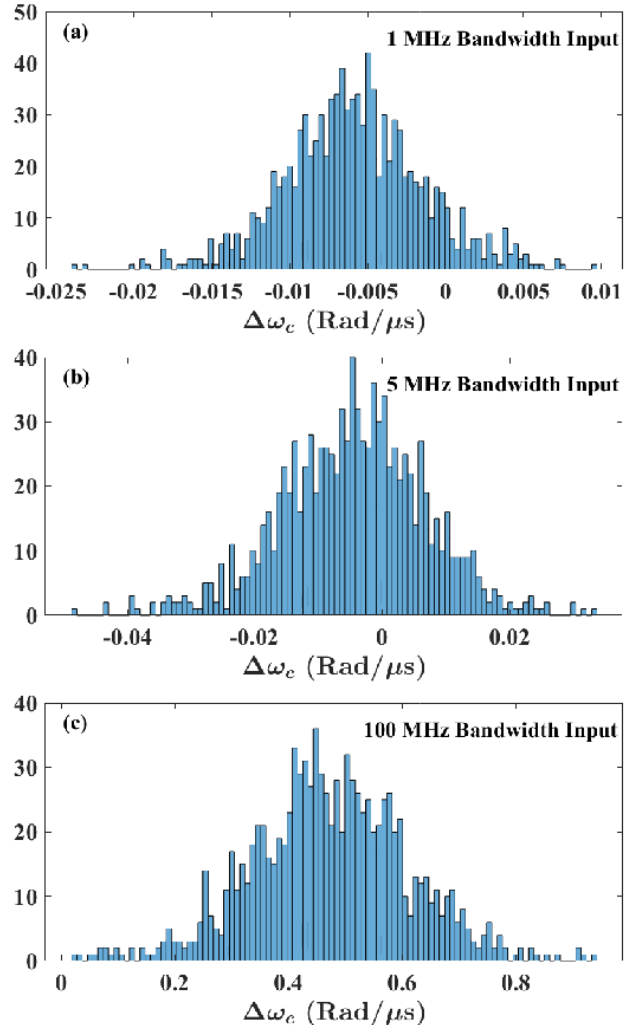


FIG. 7. Histograms of  $\Delta\omega_c$  values measured using the setup in Fig. 6(a). Each histogram consists of 1000  $\Delta\omega_c$  values. The center frequency of the pulse used in each plot is 5.23 GHz. Plots (a-c) are for the cases where the input Gaussian pulse has a bandwidth of 1 MHz, 5 MHz, and 100 MHz respectively.

## B. Errors arising from differences in time domain and frequency domain experimental setups

In Fig. 4 (b) and (c) of the main text we see that there is excellent agreement between  $D_t$  and  $\Delta t_c$ , and  $D_\omega$  and  $\Delta\omega_c$  when the system is experiencing a strong Feshbach resonance. In between these resonant regions deviations are observed between  $D_t$  and  $\Delta t_c$ , and  $D_\omega$  and  $\Delta\omega_c$ , where the time domain quantities  $\Delta t_c$  and  $\Delta\omega_c$  exhibit oscillatory behavior, but the corresponding  $D_t$  and  $D_\omega$  quantities derived from calibrated frequency-domain data do not. This behavior has a systematic frequency dependence as shown in Fig. 5, where at lower frequencies there are less of these oscillations present.

Recall, that  $D_t$  and  $D_\omega$  are essentially found by calculating the real and imaginary parts of transmission time

delay. Transmission time delay is calculated directly from the scattering matrix of the system. The scattering matrix of this system is measured in the frequency domain using a network analyzer, see Fig. 1(b) of the main text for a depiction of this measurement setup. It is imperative to note that in this measurement setup the effects of the coaxial cables (that are connecting the ring graph to the network analyzer) are calibrated out using a calibration kit. Thus, the system being measured in the frequency domain is just the ring graph.

On the other hand,  $\Delta t_c$  and  $\Delta\omega_c$  are found by calculating the shifts in transmission time and center frequency of Gaussian pulses as they traverse the graph. These measurements are performed in the time domain using a signal generator and an oscilloscope, see Fig. 6(c) for an illustration of this setup. For these time domain measurements there is no calibration kit or process that can calibrate out the effects of the external input/output coaxial cables that connects the ring graph to the measurement equipment. Thus, the system being measured is the ring graph plus the input and output cables.

We believe that the discrepancies we see between our frequency domain and time domain derived data in these in-between resonance regions are a result of the fact that the external cabling cannot be calibrated during the time domain measurements. We were able to confirm these suspicions using both simulation and experiment.

The simulation was modified to include the external cables, as shown in Fig. 8. The model consists of two ports, the ring graph, and the two external coaxial cables. Note that the ring graph and ports are identical to those utilized in Fig. 1. The two external cables attached to either side of the ring graph are simulated using the following parameters. They each have a length of 24 inches (61 cm). This is the length of the external cabling used in the experiments. The diameter of the inner and outer conductors are set to 0.0691 cm and 0.205 cm respectively. The relative permittivity of the medium is set to 1.7. The dielectric loss tangent of the medium is set to 0.00005. Lastly, the metal resistivity (normalized to gold resistivity) is set to 1.52. These values were found or estimated using data sheets for the cables used in our experiment.

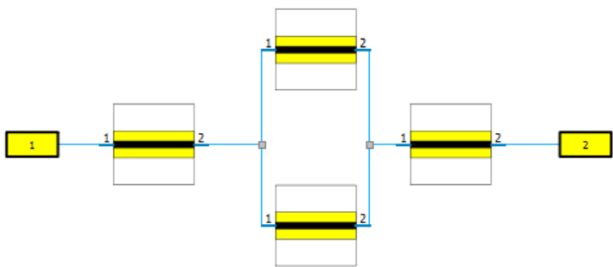


FIG. 8. CST simulation model for the case where external cabling is taken into account. Note that the ring graph is identical to the one shown in Fig. 1.

The main results of this simulation for the center-frequency shift are shown in Fig. 9. The red dots are from Fig. 2(b), while the results from the CST simulation with the external cables (Fig. 8) are plotted as well in cyan. The input Gaussian pulses have a bandwidth of 5 MHz. Here we can clearly see that near the strong resonant frequencies ( $\sim 0.72$  GHz and  $\sim 1.08$  GHz) both simulations follow the  $D_\omega$  curve well. In the “in-between” regions, we see that the cyan curve corresponding to the CST model that takes into account the external cabling has strong oscillations. These oscillations are comparable in character and amplitude to those seen in Fig. 4(d) of the main text. Again note that the CST model that does not take into account the external cabling completely lacks these oscillations.

Thus we propose that the systematic oscillations seen in the  $\Delta\omega_c$  data in the experiment arise from standing waves on the input and output cabling. The observed systematic oscillations generally have a periodicity in frequency of approximately 100 MHz. Considering a cable of length 24 inches (61 cm), one would expect a half-wave resonance to occur every 174 MHz. Two such cables will likely produce a pair of such extra resonances, leading to periodicity on the scale of roughly 87 MHz, very much comparable to the data.

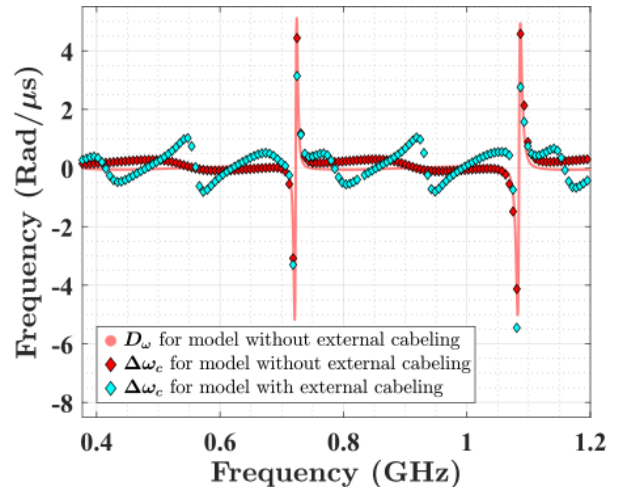


FIG. 9. Plot comparing calculated center-frequency shifts for the CST model without external cabling (Fig. 1) in red with calculated frequency shifts for the CST model with external cabling (Fig. 8) in cyan. Also shown as a solid light-red line is the predicted center frequency shift  $D_\omega$  from the CST model without external cabling.

In addition to these CST simulations, we also performed an uncalibrated scattering parameter measurement, and used the experimental  $S^{\text{NoCal}}(\omega)$  data to calculate  $D_\omega^{\text{NoCal}}$ . These results are shown in Fig. 10 and are plotted in cyan. Here we see a clear correspondence between the “deviations” in the time domain  $\Delta\omega_c$  and  $D_\omega^{\text{NoCal}}$ . This is emphasized by the zoomed-in sub-plot. This measurement provides further evidence that the systematic oscillations seen in the  $\Delta\omega_c$  data as a function

of pulse center frequency is due to standing waves on the un-calibrated input and output cables.

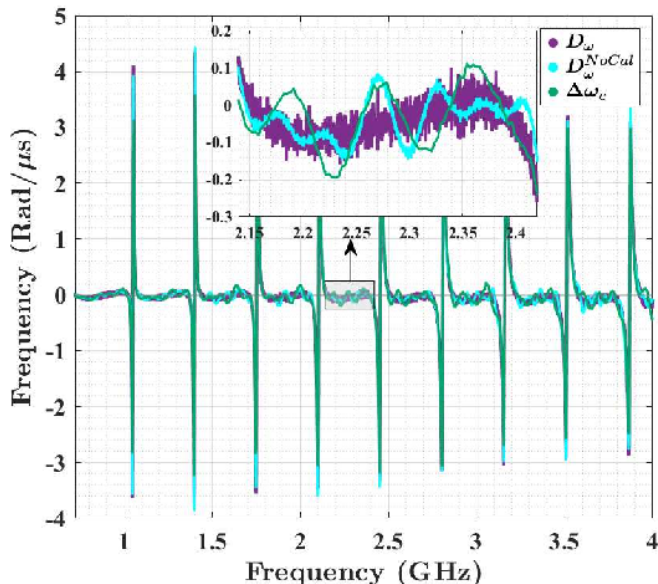


FIG. 10. Center-frequency shift data for the case where the input Gaussian pulse has a bandwidth of 5 MHz. In purple,  $D_\omega$  is plotted where the external cabling is calibrated out during the frequency domain measurement. In cyan,  $D_\omega^{\text{NoCal}}$  is plotted where the external cabling is not calibrated out. Lastly, in green is the time domain data  $\Delta\omega_c$  where the external cabling cannot be calibrated out. The inset is a zoomed-in region, of the outer plot, illustrating how  $\Delta\omega_c$  better follows  $D_\omega^{\text{NoCal}}$ .

## VII. FURTHER BACKGROUND INFORMATION ABOUT COMPLEX TIME DELAY

Here we are concerned with the presence of loss (or gain) in the system, resulting in a non-Hermitian Hamiltonian and a sub-(super-)unitary scattering matrix. Early theoretical attempts to extend time delay to non-unitary scattering systems related real time delay to the unitary deficit of the S-matrix, [6, 7] and discussed changes to the statistical distribution of the real time delay in over-moded systems [8]. However, such systems require a complex generalization of time delay to include the fact that both the phase and the magnitude of the eigenvalues of the S-matrix vary with energy.

Hints of complex time delay can be found in the use of generalized Wigner-Smith operators to find the ‘principal modes’ of complicated scattering systems, such as multi-mode optical fibers, [9, 10] particle-like scattering states in multi-mode waveguides, [11, 12] and the storage of wave energy in long-lived states in disordered media [13]. The first explicitly-articulated definition of a complex generalization of time delay for generic non-Hermitian systems appears to be the work of Asano, *et al.*, [3] who

consider the complex transmission time delay  $\tau_T$  of a simple scattering system. They consider the propagation of a Gaussian pulse through a waveguide coupled to a ring resonator and show theoretically that  $Re[\tau_T]$  describes the time-shift of the center of the pulse, and  $Im[\tau_T]$  describes the change in carrier frequency of the pulse after propagating through the system. They demonstrated experimentally the predicted results for  $Re[\tau_T]$  are correct, but did not address the predictions for  $Im[\tau_T]$ .

More recently, other researchers have embraced the complex generalization of time delay, finding it useful for description of transmission through disordered media, [14] where it has been noted that a complex transmission zero leads to a divergence of complex time delay [15, 16]. More generally, coherent perfect absorption (CPA), [17] bringing a complex zero of the S-matrix to the real frequency axis, [16–22] has as its signature the divergence of the Wigner-Smith time delay [21, 23]. Complex time delay can be directly related to the poles and zeros of the non-unitary S-matrix in the complex frequency plane [21, 24–26].



- 
- [1] D. Waltner and U. Smilansky, Scattering from a ring graph - a simple model for the study of resonances, *Acta Physica Polonica A* **124**, 1087 (2013).
- [2] D. Waltner and U. Smilansky, Transmission through a noisy network, *Journal of Physics A: Mathematical and Theoretical* **47**, 355101 (2014).
- [3] M. Asano, K. Y. Bliokh, Y. P. Bliokh, A. G. Kofman, R. Ikuta, T. Yamamoto, Y. S. Kivshar, L. Yang, N. Imoto, Ş. K. Özdemir, and F. Nori, Anomalous time delays and quantum weak measurements in optical microresonators, *Nature Communications* **7**, 13488 (2016).
- [4] H. Cao, A. Dogariu, and L. Wang, Negative group delay and pulse compression in superluminal pulse propagation, *IEEE Journal of Selected Topics in Quantum Electronics* **9**, 52 (2003).
- [5] M. A. I. Talukder, Y. Amagishi, and M. Tomita, Superluminal to subluminal transition in the pulse propagation in a resonantly absorbing medium, *Physical Review Letters* **86**, 3546 (2001).
- [6] E. Doron, U. Smilansky, and A. Frenkel, Experimental demonstration of chaotic scattering of microwaves, *Physical Review Letters* **65**, 3072 (1990).
- [7] A. Grabsch, Distribution of the wigner-smith time-delay matrix for chaotic cavities with absorption and coupled coulomb gases, *Journal of Physics A: Mathematical and Theoretical* **53**, 025202 (2019).
- [8] D. V. Savin and H.-J. Sommers, Delay times and reflection in chaotic cavities with absorption, *Phys. Rev. E* **68**, 036211 (2003).
- [9] S. Fan and J. M. Kahn, Principal modes in multimode waveguides, *Optics Letters* **30**, 135 (2005).
- [10] W. Xiong, P. Ambichl, Y. Bromberg, B. Redding, S. Rotter, and H. Cao, Spatiotemporal Control of Light Transmission through a Multimode Fiber with Strong Mode Coupling, *Physical Review Letters* **117**, 053901 (2016).
- [11] B. Gérardin, J. Laurent, P. Ambichl, C. Prada, S. Rotter, and A. Aubry, Particlelike wave packets in complex scattering systems, *Physical Review B* **94**, 014209 (2016).
- [12] J. Böhm, A. Brandstötter, P. Ambichl, S. Rotter, and U. Kuhl, In situ realization of particlelike scattering states in a microwave cavity, *Physical Review A* **97**, 021801 (2018).
- [13] M. Durand, S. M. Popoff, R. Carminati, and A. Goetschy, Optimizing light storage in scattering media with the dwell-time operator, *Physical Review Letters* **123**, 243901 (2019).
- [14] Y. Kang and A. Z. Genack, Transmission zeros with topological symmetry in complex systems, *Phys. Rev. B* **103**, L100201 (2021).
- [15] Y. Huang, Y. Kang, and A. Z. Genack, Wave excitation and dynamics in non-Hermitian disordered systems, *Physical Review Research* **4**, 013102 (2022).
- [16] P. del Hougne, K. B. Yeo, P. Besnier, and M. Davy, On-demand coherent perfect absorption in complex scattering systems: Time delay divergence and enhanced sensitivity to perturbations, *Laser & Photonics Reviews* **15**, 2000471 (2021).
- [17] Y. D. Chong, L. Ge, H. Cao, and A. D. Stone, Coherent perfect absorbers: Time-reversed lasers, *Phys. Rev. Lett.* **105**, 053901 (2010).
- [18] L. Chen, T. Kottos, and S. M. Anlage, Perfect absorption in complex scattering systems with or without hidden symmetries, *Nature Communications* **11**, 5826 (2020).
- [19] M. F. Imani, D. R. Smith, and P. del Hougne, Perfect absorption in a disordered medium with programmable meta-atom inclusions, *Advanced Functional Materials* **30**, 2005310 (2020).
- [20] B. W. Frazier, T. M. Antonsen, S. M. Anlage, and E. Ott, Wavefront shaping with a tunable metasurface: Creating cold spots and coherent perfect absorption at arbitrary frequencies, *Phys. Rev. Res.* **2**, 043422 (2020).
- [21] J. Erb, D. Shrekenhamer, T. Sleasman, T. Antonsen, and S. Anlage, Control of the scattering properties of complex systems by means of tunable metasurfaces, *Acta Physica Polonica A ISSN 1898-794X* **144**, 421 (2024).
- [22] J. Erb, N. Shaibe, R. Calvo, D. Lathrop, T. Antonsen, T. Kottos, and S. M. Anlage, Novel topology and manipulation of scattering singularities in complex non-hermitian systems (2024), arXiv:2411.01069 [cond-mat.mes-hall].
- [23] H. Li, S. Suwunnarat, R. Fleischmann, H. Schanz, and T. Kottos, Random matrix theory approach to chaotic coherent perfect absorbers, *Phys. Rev. Lett.* **118**, 044101 (2017).
- [24] L. Chen, S. M. Anlage, and Y. V. Fyodorov, Generalization of wigner time delay to subunitary scattering systems, *Phys. Rev. E* **103**, L050203 (2021).
- [25] M. Osman and Y. V. Fyodorov, Chaotic scattering with localized losses: S-matrix zeros and reflection time difference for systems with broken time-reversal invariance, *Physical Review E* **102**, 012202 (2020).
- [26] L. Chen and S. M. Anlage, Use of transmission and reflection complex time delays to reveal scattering matrix poles and zeros: Example of the ring graph, *Phys. Rev. E* **105**, 054210 (2022).